

Efficient gPC-based quantification of probabilistic robustness for systems in neuroscience

Uros Sutulovic¹, Daniele Proverbio¹, Rami Katz¹, and Giulia Giordano¹

¹Department of Industrial Engineering, University of Trento, Trento 38123, IT

February 25, 2025

Abstract

Robustness analysis is very important in biology and neuroscience, to unravel behavioral patterns of systems that are conserved despite large parametric uncertainties. To make studies of probabilistic robustness more efficient and scalable in addressing complex neuroscience models, we propose an alternative to computationally expensive Monte Carlo (MC) methods by introducing and analysing the generalised polynomial chaos (gPC) framework for uncertainty quantification. We consider both intrusive and non-intrusive gPC approaches, which turn out to be scalable and allow for a fast comprehensive exploration of parameter spaces. Focusing on widely used models of neural dynamics as case studies, we explore the trade-off between efficiency and accuracy of gPC methods, and we select effective computational settings to investigate parametric uncertainties in models that feature multiple dynamic regimes.

1 Introduction and Motivation

Systems biology [1] employs methods from mathematics, physics and engineering to understand, predict and control biological systems at all scales. Of great relevance to such efforts is the study of robustness [2, 3]. Natural systems showcase an impressive complexity; yet, they manage to thrive despite large uncertainties, variability, or external perturbations. Examples include cell homeostasis [4], multicellular coordination [5], and robust neural modulation [6]. Structural analysis [7] and robustness analysis [8] offer tools to systematically guarantee that a property of interest is preserved regardless of parameter values, or for all parameter values within a certain set. However, sometimes a property of interest does not hold structurally, nor robustly, but with some probability that one is interested in quantifying.

Probabilistic robustness has been fruitfully introduced and investigated in engineering [9], to characterise the likelihood of a system property to hold, given the probability distribution of model parameters, and to synthesise controllers that achieve a desired objective with arbitrarily high probability; here we focus however on the *analysis* of natural systems, and not on control synthesis. The most commonly used method for probabilistic analysis is Monte Carlo (MC), running many simulations with sampled random variables and corresponding random process realisations. However, MC methods suffer from poor scalability and require extensive computational power and time to gain information about even relatively simple models. Developing flexible and efficient alternative methods to quantify probabilistic robustness would scale up the investigation of parametric uncertainties in complex models, allow the extensive exploration of large parameter spaces, and enable wider adoption of robustness analysis even when low computational power must be used.

To address these challenges, we propose the use of generalised polynomial chaos (gPC), a spectral decomposition-based method to approximate the solution of differential equations with parametric uncertainties, where the uncertainties are aimed at capturing the degree of confidence of the modeller about the actual parameter values. First developed in the realm of uncertainty quantification [10, 11], gPC also found applications in other fields, such as model predictive control for stochastic systems [12], to replace or accelerate MC methods. Analysing uncertain systems by means of gPC is computationally efficient [13] and the investigation of large parameter spaces can be drastically accelerated.

Here, we systematically analyse the performance of gPC methods in providing efficient surrogate models for complex dynamical systems, with a specific focus on widely used models from neuroscience, which provide a challenging case study since they display multiple regimes (i.e., different long-term behaviors of solutions) depending on the chosen parameters. After presenting the theoretical background on gPC methods, we assess their performance and advantages over Monte Carlo approaches in terms of computing efficiency and accuracy, using several case studies from neuroscience. Finally, we employ gPC to assess the persistence of neuronal signalling regimes subject to parametric uncertainties in three models for neural dynamics, representative of different classes: the Hindmarsh-Rose model (semi-phenomenological model for single-neuron dynamics), the Jansen-Rit model (mechanistic model for multiple connected neurons), and the Epileptor model (phenomenological model for epileptic activity in brain regions).

2 Problem Formulation and Background

We consider autonomous ODE systems of the form

$$\dot{\mathbf{x}} = f(\mathbf{x}, Z), \quad (1)$$

where $\mathbf{x} \in \mathbb{R}^n$ is the state of the system and $Z \in \mathbb{R}^d$ is a parametric uncertainty. Differently from stochastic differential equations, where the dynamics are driven by a stochastic process, our source of stochasticity is induced by parametric uncertainties, i.e., we assume that $Z: \Omega \rightarrow I_Z \subset \mathbb{R}^d$ is a vector of mutually-independent random variables defined on some probability space $(\Omega, \mathcal{F}, \mathbb{P})$, where Ω denotes a sample space containing samples $\omega \in \Omega$, $\mathcal{F} \subset 2^\Omega$ is a σ -algebra and \mathbb{P} is a probability measure. We assume that Z is absolutely continuous with respect to the Lebesgue measure, and denote its probability density function (PDF) by $\rho_Z(z)$.

Remark If the random variables Z are not mutually independent, the Rosenblatt transformation [14] can be applied to transform them into new, mutually independent random variables \tilde{Z} . Hence, from a theoretical perspective, assuming mutual independence poses no loss of generality. \diamond

Due to the parametric uncertainty, the state in (1) is a stochastic process $\mathbf{x}(t; Z)$. Characterizing the first moments (summary statistics) of $\mathbf{x}(t; Z)$, for example in order to approximate its characteristic function [15], is of interest.

The estimation of summary statistics is often performed by a combination of explicit formulas (available only in rare cases) and randomised algorithms. Monte Carlo methods are widely used in computational studies, to perform random sampling for numerical simulations and extraction of summary statistics. Yet, they may be impractical when simulating large models with uncertain parameters: their sample complexity scales poorly with model dimensionality, and grows rapidly with increase in the desired accuracy [9].

To overcome such complexity limitations, alternative surrogate models need to be identified, that are computationally more tractable and sufficiently accurate. For practical applications, it is also necessary to determine, at least empirically, *how well* such surrogate models perform in uncertainty quantification and robustness analysis tasks. Here we propose the use of various gPC methods to estimate summary statistics.

Table 1: Wiener-Askey scheme

PDF of Z	Basis $\{\Phi_\alpha\}_\alpha$
Gaussian	Hermite polynomials
Uniform	Legendre polynomials
Beta	Jacobi polynomials
Gamma	Laguerre polynomials

2.1 Generalised polynomial chaos

Considering the probability density function of Z in (1), we restrict our attention to the set of functions $\psi: I_Z \rightarrow \mathbb{R}$ that belong to the weighted L^2 space

$$L_{\rho_Z}^2(I_Z) = \left\{ \psi : \mathbb{E}[\psi^2] = \int_{I_Z} \psi^2(z) \rho_Z(z) dz < \infty \right\}. \quad (2)$$

A natural basis for the space $L_{\rho_Z}^2(I_Z)$ is a set of multivariate polynomials $\{\Phi_\alpha(z)\}_\alpha$ satisfying the orthogonality relation

$$\mathbb{E}[\Phi_\alpha \Phi_\beta] = \int_{I_Z} \Phi_\alpha(z) \Phi_\beta(z) \rho_Z(z) dz = \gamma_\alpha \delta_{\alpha\beta}, \quad (3)$$

where $\gamma_\alpha = \mathbb{E}[\Phi_\alpha^2] > 0$ is a normalizing factor, and $\delta_{\alpha\beta}$ is the d -variate Kronecker delta. Here, $\alpha = (\alpha_1, \dots, \alpha_d) \in \mathbb{N}_0^d$ is a multi-index. The basis $\{\Phi_\alpha(z)\}_\alpha$ can be obtained from a Gram-Schmidt orthogonalisation process applied to the set of monomials $\{\prod_{i=1}^d z_i^{\alpha_i}\}_{\alpha \in \mathbb{N}_0^d}$. Henceforth, we assume that $\gamma_\alpha = 1$ for all $\alpha \in \mathbb{N}_0^d$, meaning that the polynomials $\{\Phi_\alpha(z)\}_\alpha$ are orthonormal.

Wiener [16] proved a PC expansion for a normally distributed $Z \sim N(\mathbf{0}, I)$:

$$\psi(Z) = \sum_{|\alpha|=0}^{\infty} \hat{\psi}_\alpha \Phi_\alpha(Z), \quad \hat{\psi}_\alpha = \mathbb{E}[\psi \Phi_\alpha], \quad (4)$$

where $\{\Phi_\alpha(z)\}_\alpha$ is a base of Hermite polynomials and $|\alpha| = \sum_{i=1}^d \alpha_i$. Later, Cameron and Martin [17] generalised this expansion to random variables Z with an arbitrary distribution. Xiu and Karniadakis [11] proposed a framework that links standard random variables and their densities to the corresponding orthogonal polynomials of the Wiener-Askey table, some of which are given in Table 1. Constructing the basis $\{\Phi_\alpha(z)\}_\alpha$ in case of arbitrarily distributed random variables is the subject of dedicated studies; for instance, we refer to the procedures described in [18].

For the stochastic process $\mathbf{x} = \mathbf{x}(t; Z)$, subject to the dynamics in (1), the gPC expansion reads

$$\begin{aligned} \mathbf{x}(t; Z) &= \sum_{\alpha \in \mathbb{N}_0^d} \hat{\mathbf{x}}_\alpha(t) \Phi_\alpha(Z), \\ \hat{\mathbf{x}}_\alpha(t) &= [\hat{\mathbf{x}}_{\alpha,1}(t) \dots \hat{\mathbf{x}}_{\alpha,n}(t)]^\top \in \mathbb{R}^n, \\ \hat{\mathbf{x}}_{\alpha,j}(t) &:= \mathbb{E}[\mathbf{x}_j(t, \cdot) \Phi_\alpha], \quad j = 1, \dots, n. \end{aligned} \quad (5)$$

Intuitively, gPC methods represent the stochastic process $\mathbf{x}(t; Z)$ as a series expansion with respect to an appropriate basis of orthogonal polynomials depending on the uncertain parameters Z and the corresponding density ρ_Z , with coefficients depending on time t , as in equation (5). The spectral coefficients $\{\hat{\mathbf{x}}_\alpha(t)\}_\alpha$ contain all the temporal information, while the stochasticity is confined in the orthogonal polynomials $\{\Phi_\alpha(Z)\}_\alpha$, thereby achieving separation of the stochastic and deterministic elements that define the dynamics. The relation (3) and the linearity of the spectral representation (5) can thus be used to compute the summary statistics of $\mathbf{x}(t; Z)$. For arbitrary statistical moments, we refer the reader to [19]. In this work we only consider mean and variance, extracted as

$$\mu_{\mathbf{x}}(t) = \hat{\mathbf{x}}_0(t) \quad \text{and} \quad \sigma_{\mathbf{x}}^2(t) = \sum_{|\alpha| \neq 0} \hat{\mathbf{x}}_\alpha^2(t). \quad (6)$$

The expansion (5) holds theoretically; in practice, for numerical implementation, it must be truncated to obtain a finite-sum approximation that can be substituted into the expression of the statistical moments in equations (6). Finite-sum approximations can be computed either by intrusive approaches (e.g. Galerkin), which modify the governing equations of the original system by truncating the gPC expansion, or by non-intrusive approaches (e.g. collocation) that treat the model as a black box and use sampling to estimate the spectral coefficients indirectly, e.g. via least-squares regression.

As a first approach to generate an approximation of $\mathbf{x}(t; Z)$, assume (only for demonstration purposes, without loss of generality) that (1) is a polynomial system, i.e.

$$\begin{aligned} f(\mathbf{x}, Z) &= \sum_{|k| \leq L} a_k(Z) x_1^{k_1}(t, Z) \dots x_n^{k_n}(t, Z), \\ a_k(Z) &= \sum_{\alpha \in \mathbb{N}_0^d} \hat{a}_{k,\alpha} \Phi_\alpha(Z) \in \mathbb{R}^n, \end{aligned} \quad (7)$$

where $k = (k_1, \dots, k_n) \in \mathbb{N}_0^n$ and $L \in \mathbb{N}_0$. By substituting (5) and (7) into (1), multiplying both sides by Φ_β and taking the expectation, we have

$$\begin{aligned} \frac{d}{dt} \hat{\mathbf{x}}_\beta(t) &= \mathbb{E}[f(\sum_{\alpha \in \mathbb{N}_0^d} \hat{\mathbf{x}}_\alpha(t) \Phi_\alpha, Z) \Phi_\beta] \\ &= \sum_{|k| \leq L} \mathbb{E}[\chi_k \Phi_\beta], \quad \beta \in \mathbb{N}_0^d, \\ \chi_k &:= \left(\sum_{\alpha \in \mathbb{N}_0^d} \hat{a}_{k,\alpha} \Phi_\alpha \right) \prod_{j=1}^n \left(\sum_{\alpha \in \mathbb{N}_0^d} \hat{\mathbf{x}}_{\alpha,j}(t) \Phi_\alpha \right)^{k_j}. \end{aligned} \quad (8)$$

The approximation to $\mathbf{x}(t; Z)$ is then of the form

$$\begin{aligned} \mathbf{x}_N(t; Z) &= \sum_{|\alpha| \leq N} \tilde{\mathbf{x}}_\alpha(t) \Phi_\alpha(Z), \\ \tilde{\mathbf{x}}_\alpha(t) &= [\tilde{\mathbf{x}}_{\alpha,1}(t) \quad \dots \quad \tilde{\mathbf{x}}_{\alpha,n}(t)]^\top \in \mathbb{R}^n, \end{aligned} \quad (9)$$

where the coefficients $\{\tilde{\mathbf{x}}_i(t)\}_{|\alpha| \leq N}$ in (9) are obtained as solutions to the truncated system:

$$\begin{aligned} \frac{d}{dt} \tilde{\mathbf{x}}_\beta(t) &= \sum_{|k| \leq L} \mathbb{E}[\tilde{\chi}_k \Phi_\beta], \quad |\beta| \leq N, \\ \tilde{\chi}_k &:= \left(\sum_{|\alpha| \leq N} \hat{a}_{k,\alpha} \Phi_\alpha \right) \prod_{j=1}^n \left(\sum_{|\alpha| \leq N} \tilde{\mathbf{x}}_{\alpha,j}(t) \Phi_\alpha \right)^{k_j}. \end{aligned} \quad (10)$$

System (10) is obtained from system (8) by retaining only polynomials whose degree is less or equal to N . This approach is the so-called stochastic Galerkin projection.

A competing approach to generate surrogates of $\mathbf{x}(t; Z)$ is the collocation method, based on sampling the values of the random variable Z . Let $\{Z^{(j)}\}_{j=1}^{S_C} \subset I_Z$, $S_C \geq \binom{N+d}{d}$, be a grid of nodes sampled in the range of Z . There are multiple ways to generate such a grid – as pseudo-random Monte Carlo sampling according to ρ_Z , as nodes of a pre-selected quadrature rule, the Smolyak sparse grid [20] or a Clenshaw-Curtis grid [21]. For each $1 \leq j \leq S_C$, let $\bar{\mathbf{x}}^{(j)}(t)$ be a solution to the *deterministic* system (1) with Z replaced by the value $Z^{(j)}$. The desired approximation to $\mathbf{x}(t; Z)$ is considered again in the form (9), subject to the interpolation conditions

$$\mathbf{x}_N(t; Z^{(j)}) = \sum_{|\alpha| \leq N} \tilde{\mathbf{x}}_\alpha(t) \Phi_\alpha(Z^{(j)}) = \bar{\mathbf{x}}^{(j)}(t) \quad (11)$$

where $1 \leq j \leq S_C$. These conditions impose an over-determined (due to the condition on S_C) linear system on the coefficients $\{\tilde{\mathbf{x}}_\alpha(t)\}_{|\alpha| \leq N}$, which can be solved either explicitly or via a least-squares projection.

Remark The collocation procedure has the same form regardless of the structure of the dynamics. Conversely, the Galerkin approach can be made more precise for polynomial systems when expectations of higher order products of basis elements are explicitly available [22], and can be embedded in (10), without any additional approximation (such as cubature formulas for integral approximations). \diamond

The rate of convergence of the approximation of a static map $f(Z) = \sum_{\alpha \in \mathbb{N}_0^d} f_\alpha \Phi_\alpha(Z)$ depends on the smoothness of f and the type of orthogonal polynomial basis functions $\{\Phi_\alpha\}_\alpha$ employed in the approximation [23]. For $f \in H_{\rho_Z}^\ell(I_Z) \subset L_{\rho_Z}^2(I_Z)$ (i.e., f is in an appropriate

Sobolev space), the approximation error $\|f - \sum_{|\alpha| \leq N} f_\alpha \Phi_\alpha\|_{L^2_{\rho_Z(I_Z)}}$ is $\mathcal{O}(N^{-\ell})$. For analytic f , the convergence rate is exponential, i.e. $\mathcal{O}(e^{-\sigma N})$ for some constant $\sigma > 0$. For solutions to ODE systems (1), few rigorous results that quantify the convergence rates exist. Some analytic results and numerous numerical studies found in the literature indicate that similar convergence rates hold for $\|\mathbf{x}(t; \cdot) - \mathbf{x}_N(t; \cdot)\|_{L^2_{\rho_Z}(I_Z)}$, at least on compact time intervals; see [12, 11] for further details.

As analytical and generic frameworks are missing to estimate the convergence of gPC methods on general systems and to compare them with Monte Carlo convergence results, numerical investigation should be employed to gain insight as to how gPC compares with MC methods. Such numerical comparisons have been explored rarely and only few case-specific results are available, especially for systems in biology [24], where Monte Carlo has been the main workhorse for decades. To perform a detailed comparison of gPC variants and Monte Carlo methods in neuroscience models, characterised by different operating regimes emerging from their dynamics, we consider as case studies the Hindmarsh-Rose model for single-neuron dynamics, the Jansen-Rit model for collective neural dynamics, and the Epileptor model for epilepsy.

2.2 The Hindmarsh-Rose (HR) model

The Hindmarsh-Rose (HR) model [25] captures the dynamics of action-potential within a single neuron capable of bursting activity [26]. It can display numerous patterns of trajectory behaviours, ranging from cyclic spiking to bursting or chaos, depending on the considered parameter sets [27], which are often uncertain due to experimental design or neural activity. The corresponding (non-dimensionalised) set of ODEs is:

$$\begin{cases} \dot{x} = y - ax^3 + bx^2 - z + I, \\ \dot{y} = c - dx^2 - y, \\ \dot{z} = r[s(x - x_R) - z], \end{cases} \quad (12)$$

where x represents membrane potential, y is a fast recovery current, z is a slow adaptation current; I is an externally applied current (either experimental current injection or in-vivo synaptic current), and the other terms are model parameters. Their values can be inferred from fitting the model to experimental data [28], and may depend on the considered organism and come with significant uncertainties. If parameter values are changed *deterministically*, bifurcation studies [29, 30] allow to identify parameter combinations corresponding to various patterns.

Fixing a, c, d, r, s and x_R in (12) to default values $a = 1, b = 3, c = 1, d = 5, r = 0.01, s = 4, x_R = -8/5$, and letting $I \in [2.2; 4.4]$ and $b \in [2.5; 3.3]$ vary within the given intervals, five dynamical regimes can be recognised in the HR dynamics [31, 29, 30]: (A) quiescence, (B) tonic spiking, (C) square-wave bursting, (D) plateau bursting and (E) chaotic bursting. See the illustration in Fig. 1.

2.3 The Jansen-Rit (JR) model

The Jansen-Rit model [32] is a neural mass model explaining dynamics of interconnected neuronal populations of different neural types (pyramidal cells and inhibitory and excitatory interneurons in the cortical area). Similarly to HR, it can exhibit behaviors like quiescence, chaos, and periodic and quasi-periodic patterns for biologically plausible parameter ranges. The model is given by [32]:

$$\begin{cases} \dot{y}_1 = y_4; \quad \dot{y}_2 = y_5; \quad \dot{y}_3 = y_6 \\ \dot{y}_4 = A a S(y_2 - y_3) - 2a y_4 - a^2 y_1 \\ \dot{y}_5 = A a [p + C_2 S(C_1 y_1)] - 2a y_5 - a^2 y_2 \\ \dot{y}_6 = B b C_4 S(C_3 y_1) - 2b y_6 - b^2 y_3, \end{cases} \quad (13)$$

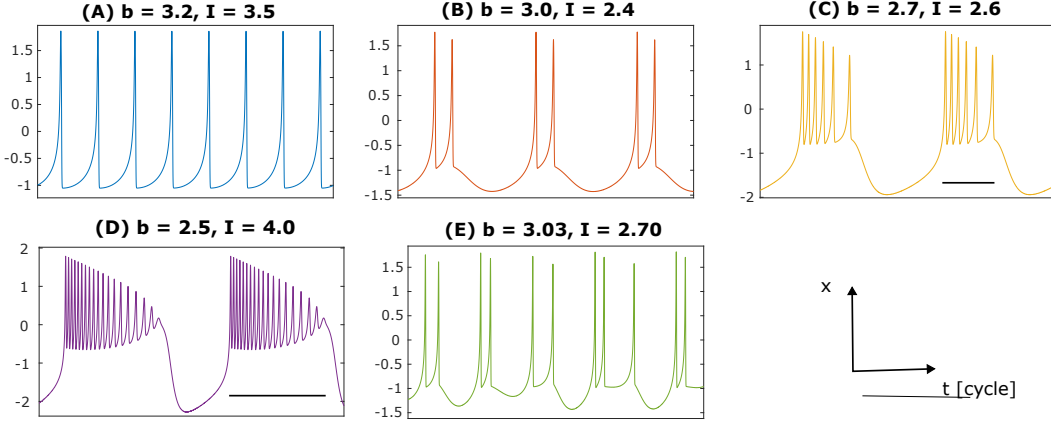


Figure 1: Examples of time series $x(t)$ for the regimes (A)–(E) of the HR model (12), described in the main text. The lines in (C) and (D) identify a burst of spikes.

where $S(V) = \nu_M / (1 + e^{r(V_0 - V)})$, with ν_M being the maximal firing rate of the family of neurons and V_0 the excitability threshold of the population; r is the “firing threshold variance”, i.e., the slope of the sigmoid at V_0 . The connectivity constants C_i in (13) are all proportional to a single parameter C [32]: $C_1 = C$, $C_2 = 0.8C$, $C_3 = 0.25C$, $C_4 = 0.25C$. Variables y_i represent neural potentials, and the other model parameters are usually fixed to reproduce basic properties of postsynaptic potentials and cortical activity. Typical values, which we employ for simulations, are $C = 135$, $A = 3.25\text{ mV}$, $B = 22\text{ mV}$, $a = 100\text{ s}^{-1}$, $b = 50\text{ s}^{-1}$, $V_0 = 6\text{ mV}$, $\nu_{max} = 5\text{ s}^{-1}$, $r = 0.56\text{ mV}^{-1}$; p is usually uncertain within a maximum interval $[0; 400]\text{ s}^{-1}$.

2.4 The Epileptor model

The Epileptor model was introduced in [33] as a phenomenological mean field model aimed at capturing the average seizure dynamics of blocks of neurons. It expands on the HR model (12) by adding couplings to generate seizure-like events. The non-dimensionalised model is given by

$$\begin{cases} \dot{x}_1 = x_2 - f_1(x_1, x_4) - x_3 + I_1, \\ \dot{x}_2 = r_2 - 5x_1^2 - x_2, \\ \dot{x}_3 = \frac{1}{\tau_0}(4(x_1 - r_1) - x_3), \\ \dot{x}_4 = -x_5 + x_4 - x_4^3 + I_2 + 2u - 0.3(x_3 - 3.5), \\ \dot{x}_5 = \frac{1}{\tau_2}(-x_5 + f_2(x_4)), \\ \dot{u} = -\gamma(u - 0.1x_1), \end{cases} \quad (14)$$

where $(r_1, r_2, I_1, I_2) = (-1.6, 1, 3.1, 0.42)$ are the system parameters, $(\tau_0, \tau_2, \gamma) = (2857, 10, 0.01)$ are timescale constants, u is a low-pass filter “dummy variable” [33] and the non-smooth coupling functions are given by

$$\begin{aligned} f_1(x_1, x_4) &= \begin{cases} x_1^3 - 3x_1^2, & x_1 < 0, \\ (x_4 - 0.6(x_3 - 4)^2)x_1, & x_1 \geq 0, \end{cases} \\ f_2(x_4) &= \begin{cases} 0, & x_4 < -0.25, \\ 6(x_4 + 0.25), & x_4 \geq -0.25. \end{cases} \end{aligned} \quad (15)$$

Variables (x_1, x_2) govern the oscillatory behaviors, (x_4, x_5) introduce the spikes and wave components typical of seizure-like events, and x_3 is a slow permittivity variable driving the system to the seizure threshold.

2.5 Methodology

We aim to demonstrate the advantage of gPC methods in reconstructing summary statistics for individual regimes of each model. To this end, we select parameters of interest \hat{p}_i , determined from a literature overview and the biological meaning of each model, and consider uniform distributions for them, i.e., $\hat{p}_i \in [\hat{p}_{i,j}^{\min}; \hat{p}_{i,j}^{\max}]$, where j further identifies the regime. Minimum and maximum values may differ among regimes, due to their persistence set (see e.g. [34, Figure 3]). For instance, in the HR model, j identifies one of the regimes $\{A, B, C\}$ for parameter b ; for regime D , we fix b and vary $I \in [I_{\text{HR},D}^{\min}; I_{\text{HR},D}^{\max}]$ uniformly. Chaos (regime E) adds another layer of complexity and is currently not investigated. Choices of parameter ranges for the other models are described together with the subsequent results.

The computational complexity is assessed through the use of a proxy measure, the running time τ_m (where m refers to the considered surrogate method, Monte Carlo, Galerkin or collocation) on a fixed hardware (a Dell Inspiron 16 laptop with 16 GB RAM and 1.90 GHz Intel i5-1340P core, running Windows 11 and kept on charge, to avoid power saving modes). To assess the accuracy performance of gPC methods, we first construct a “benchmark” state for each model and regime, employing a Monte Carlo (MC) scheme with $N_{MC} = 10^5$ that guarantees accuracy $\varepsilon < 0.01$ for a confidence $\delta = 0.01$ [9] albeit requiring $\tau_{MC} > 7\text{h}$ for the HR model and even $\tau_{MC} > 29\text{h}$ for the Epileptor model.

Given a final simulation time T and a time-step dt , we compute the error vector between the MC-based “benchmark” and the surrogate models results $e \in \mathbb{R}^{N_e}$, $N_e = \frac{T}{dt}$. Deviations for both mean and variance are estimated using the element-wise root mean square error (RMSE)

$$e_{\text{RMS}} = \sqrt{\frac{1}{N_e} \sum_{n=1}^{N_e} e_n^2},$$

where e_n is the n th entry of vector e .

As a representative MC approximated method, we use a Monte Carlo chain with $N_{MC} = 5000$. In the subsequent analysis, we always consider its best (either the fastest or the most precise) run, among those from all considered regimes.

For the Galerkin approach, we assess the accuracy of the obtained surrogate model (9) with respect to the expansion order $N = N_G$. For the collocation approach, we assess the accuracy of the obtained surrogate model (9) with respect to both the expansion order $N = N_C$ and the number of collocation samples S_C . The time τ_m is estimated from the first call of the polynomial projection to the estimation of the statistical moment of interest. This is a worst-case time in the case of new simulations, as it includes the compilation time for the expansion polynomials, which can then be stored in the case of repeated runs without concurring to additional processing.

Simulations of all models are performed using MATLAB `ode45` function. Consistently with studies in literature, we use $dt = 0.01$ up to $T = 1200$ for the HR model, $dt = 2.5 \cdot 10^{-4}$ up to $T = 2.5$ for the JR model, and $dt = 0.01$ up to $T = 4500$ for the Epileptor model; initial conditions are set uniformly at $[0, \dots, 0]^\top$ for the HR and JR models, and at $[0, -5, 3, 0, 0, 0]^\top$ for the Epileptor model. gPC approaches are implemented via the PoCET MATLAB toolbox [22], already optimised for uncertainty quantification. To maintain consistency and fairness of comparison, Monte Carlo simulations are also performed using PoCET built-in functions.

3 Results

3.1 gPC methods outrun MC and maintain accuracy

For the HR, the rapid and approximated MC chain with $N_{MC} = 5000$ has running time in the order of 10^3 s, and mean and variance of RMSE are around 0.01.

For the Galerkin approximation, the computation time τ_G in all regimes scales sub-exponentially

for small expansion orders and exponentially for medium-large N_G , following a best fit relation

$$\tau_G = \tilde{a} e^{\tilde{b} N_G} + \tilde{c} e^{\tilde{d} N_G}, \quad (16)$$

with $\tilde{a}, \tilde{b}, \tilde{c}, \tilde{d} \in \mathbb{R}$ (see also Fig. 2a). For any considered expansion order, τ_G is at least one order of magnitude lower than τ_{MC} , marking a significant acceleration in computation. Despite fluctuations related to stochasticity, the mean RMSE decays rapidly (following the same trend as in (16), with different parameters) as the expansion order increases (Fig. 2b). For A, B the mean discrepancy with high N_G is close to that of the MC chain, while it is significantly higher for regimes with bursting, such as C and D . Overall, the variance of the RMSE remains approximately constant for increasing N_G , mostly around values of 0.3, which is about three times that of MC; see Fig. 2c. These results suggest that the Galerkin approximation drastically speeds up the computation time with respect to MC methods, but at the price of decreasing accuracy, which might be acceptable in certain applications, such as the preliminary sweeping of the parameter space in order to identify regions of interest.

Collocation relies both on expansion order N_C and on the number of collocation samples S_C . Fig. 3 shows the best-case and worst-case surfaces obtained from testing all regimes: given for each $\{N_C, S_C\}$ a vector $z(N_C, S_C) = [z_i(N_C, S_C)]$ where i denotes the regime, we show the surfaces that interpolate $\max(z)$ and $\min(z)$. For comparison, we also show the surface associated with MC values, in gray. The running time τ_C (Fig. 3a) and the mean RMSE (Fig. 3b) are more significantly influenced by the number of collocation samples, whereas the expansion order has relatively little impact, at least in the considered interval. On the other hand, a higher expansion order significantly improves the variance of the RMSE (Fig. 3c), which is consistent with (6). Notably, even for high N_C and high S_C , the running time remains around 2 minutes, while MC takes about 20 minutes, highlighting a $10\times$ acceleration. We have not considered expansion orders above $N_C > 15$, which would further slow down the computation, since the mean of the RMSE is already sufficiently close to that of MC (only twice its value), even with a relatively low expansion order N_C , at the price of losing one order of magnitude in the variance of the RMSE.

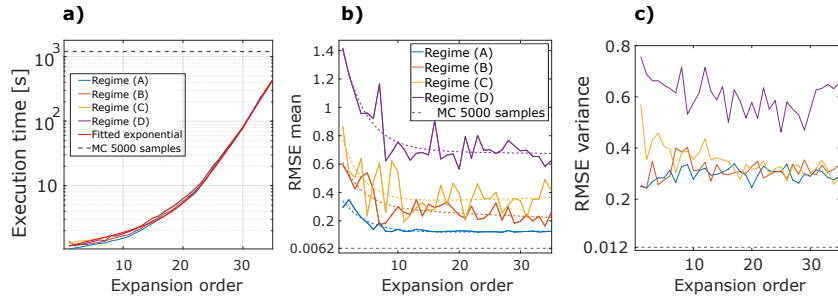


Figure 2: Results of Galerkin gPC approximation, for the considered HR regimes, depending on the expansion order N_G . The gray dashed lines represent values from the MC approximation, with $\tau_{MC} = 1238$ s, mean RMSE = 0.0062, variance RMSE = 0.012. (a) Running time τ_G . The fit example follows (16) for the regime C ; the trend is conserved for all regimes. (b) Mean of RMSE. Dashed lines represent empirical fitting from (16). (c) Variance of RMSE.

JR and Epileptor models are not polynomial. Hence, the Galerkin method is not applicable with the POCET toolbox and, to maintain consistency with the previous results, we only employ the collocation method.

For the JR model, we consider an uncertainty over the input p with uniform distribution $p \in [120; 320]$. We test different dynamical cases by setting $C = 68, C = 95, C = 128, C = 135, C = 155$ and $C = 173$, so that the dynamical regimes resemble cortical signals that are non-oscillatory, waning sinusoidal-like, sinusoidal-like and low frequency quasi-periodic; see [32, Figure 3]. Simulations with MC are rather fast, with τ_{MC} in the order of 10^2 s. Collocation, however, achieves even better performance, providing statistics with a running time below 40s. Similarly to the HR case, Fig. 4 shows the best- and worst-case surfaces for τ_C and the RMSE

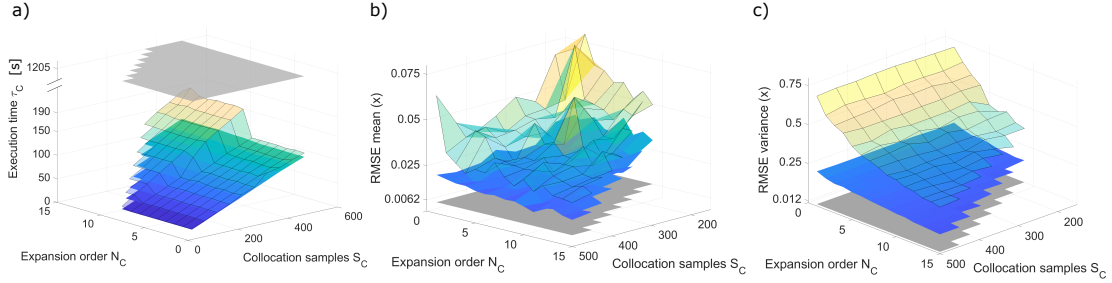


Figure 3: Results for the collocation gPC approximation for the HR model. We show the best-case and worst-case surfaces, which interpolate minimum and maximum values of τ_C and of performance metrics among all regimes, for each point $\{N_C, S_C\}$. Gray surface: values of the MC approximation, with $\tau_{MC} = 1238$ s, mean RMSE = 0.0062, variance RMSE = 0.012. (a) Running time τ_C ; note that the z-axis is cut to show the MC surface, with very high τ_C . (b) Mean of RMSE for the variable x . (c) Variance of RMSE for the variable x .

statistics. The trends are consistent with HR results: collocation speeds up the computation, and a higher number of collocation samples S_C significantly improves the RMSE mean, while the RMSE variance is mostly driven by the expansion order N_C , and decreases rapidly (for the worst-case surface) as N_C increases. Notably, the best collocation approximations are *even more accurate* than those obtained with MC; see the blue surface overlapping with the gray one in Fig. 4b,c. This fact highlights that, in some cases, the collocation method provides precise approximations for most $\{N_C, S_C\}$ combinations. The discrepancy between best-cases and worst-cases is drastically reduced by selecting $N_C > 15$ and $S_C > 500$.

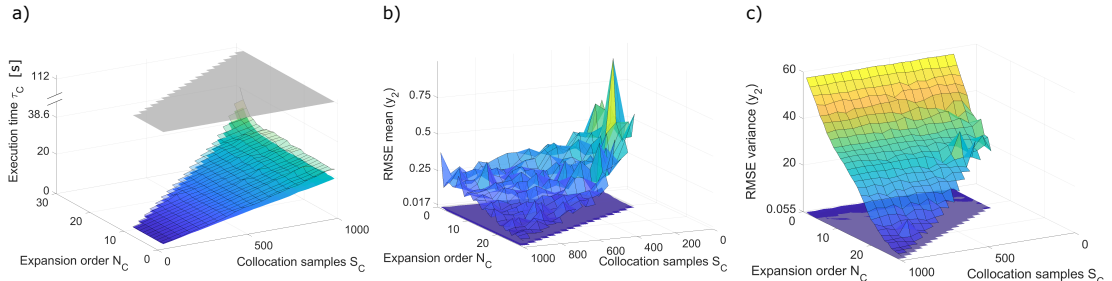


Figure 4: Results for the collocation gPC approximation for the JR model. We show the best-case and worst-case surfaces, which interpolate minimum and maximum values of τ_C and of performance metrics among all regimes, for each point $\{N_C, S_C\}$. Gray surface: values of the MC approximation, with $\tau_{MC} = 112$ s, mean RMSE = 0.017, variance RMSE = 0.055. (a) Running time τ_C ; note that the z-axis is cut to show the MC surface, with very high τ_C . (b) Mean of RMSE for the variable y_2 . (c) Variance of RMSE for the variable y_2 .

Finally, we consider the Epileptor model and specifically the single dynamical regime that reproduces seizure-like dynamics, so as to be in line with the model scope. Bounds of the uniform distribution for \hat{p}_i are thus chosen not to yield other regimes. Three different realisations to construct the vector $z(N_C, S_C)$ are obtained by considering (one at a time) uniform distributions for I_1, I_2, τ_0 while leaving other parameters at default settings. A fourth realisation uses $\hat{p}_4 = I_1$ and $I_2 = 0.2$. Since the Epileptor is complex and requires long simulations with small time steps, to capture fast discharges, spikes and wave events [33], the computing time for the MC exceeds 5000s, while the gPC collocation method requires one order of magnitude less and τ_C scales almost linearly with S_C ; see Fig. 5a. Results for the RMSE mean and variance are similar to those of the HR, as the RMSE becomes very close to that obtained with MC (twice its value) even with a relatively low expansion order N_C , at the price of losing one order of magnitude in the variance of RMSE. The analogy with the results achieved with the HR model is not surprising, as the Epileptor uses the HR model as its kernel; the main difference lies in

the low discrepancy between best- and worst-case surfaces for the RMSE variance, which is explained by the higher complexity of the Epileptor model.

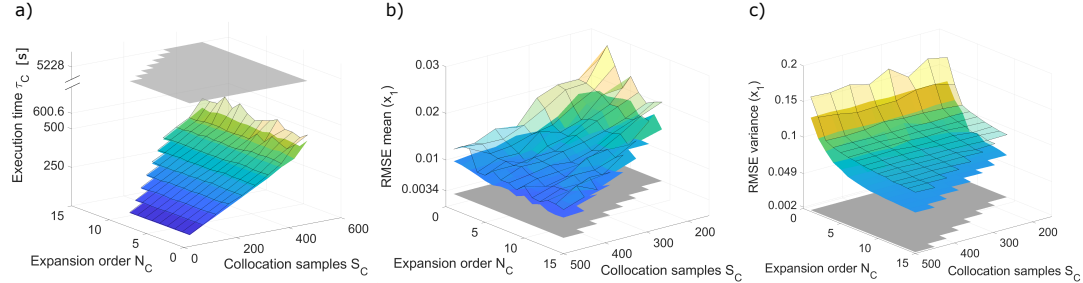


Figure 5: Results for the collocation gPC approximation for the Epileptor. We show the best-case and worst-case surfaces, which interpolate minimum and maximum values of τ_C and of performance metrics among all regimes, for each point $\{N_C, S_C\}$. Gray surface: values of the MC approximation, with $\tau_{MC} = 5228$ s, mean RMSE = 0.0062, variance RMSE = 0.012. (a) Running time τ_C ; note that the z-axis is cut to show the MC surface, with very high τ_C . (b) Mean of RMSE for the variable x_1 . (c) Variance of RMSE for the variable x_1 .

3.2 Computing probabilistic robustness

Our previous findings support the use of collocation methods to study probabilistic robustness, achieving a good compromise between computing time and accuracy of the results. With respect to Galerkin, collocation methods achieve higher accuracy in all regimes. On the other hand, MC is too computationally demanding when investigating multiple uncertainties or considering large parametric spaces (which are common in neuroscience), whereas we have demonstrated that gPC is not. To analyse pattern robustness for the HR model, we therefore employ collocation gPC. A high N_C yields better RMSE performance without losing much in terms of τ_C . For S_C , we notice in Fig. 3 that $S_C > 400$ does not improve RMSE statistics, but only increases τ_C . Hence, we select $S_C = 400$ and $N_C = 15$.

As a first case study to showcase the possibility of using gPC for probabilistic robustness, we consider a selected regime: plateau bursting (D) of the HR. For a given $I = 4.2$, we thus investigate the probability that D persists, depending on sampled values b within a uniform distribution $b \in I_b = [2.4; 2.8]$, where 2.4 is associated with typical leftmost values considered in phase planes from the literature [34], and $\Delta b = 0.4$ is informed by experimental uncertainties obtained from fitting experimental data [31]. Plateau bursting is known to be characterised by a Hopf bifurcation [29] marking the end of the burst of spikes at $x = 0$. We use this signature on the gPC mean to automatically identify if the simulations maintain regime D or not. We further characterise the proportion $P^* = \frac{\text{size}(A_b)}{\text{size}(I_b)}$, where $A_b \subseteq I_b$ is the interval for which D is preserved, as a probabilistic measure of robustness.

The gPC mean in each interval $A_b \subseteq I_b$ is immediately computed following equation (6) in PoCET. Fig. 6a shows an example of the expectation $\mu_x(t)$ for $b \in [2.4; 2.48]$, for which the burst of spikes ends at $\mu_x(t) = 0$ (red dot, when the neuron re-polarises). Fig. 6b shows an example for $b \in [2.64; 2.72]$, whose re-polarisation occurring at $\mu_x(t) < 0$ clearly indicates a signature of regime C (cf. Fig. 1), and not D . Other intervals A_b are systematically checked using the same criterion, to study the persistence of D .

We eventually identify in $A_b^* = [2.4; 2.56]$ the robust interval for regime D , corresponding to $P^* = 40\%$, which is consistent with biological studies [31] suggesting that, in experiments, square-wave bursts are more common than plateau bursting. The result for A_b^* is in line with studies in the literature using alternative methods [30, 34, 29]. The whole process took about 8.2 minutes to complete, with clear advantages over MC (recall that a *single* MC run on an arbitrary distribution of b takes around 20 minutes). Our proposed method thus allows for a

rapid analysis that is sufficient for the probabilistic quantification of persistence of a desired regime. Further refinements may be used to hone the probability estimates even further.

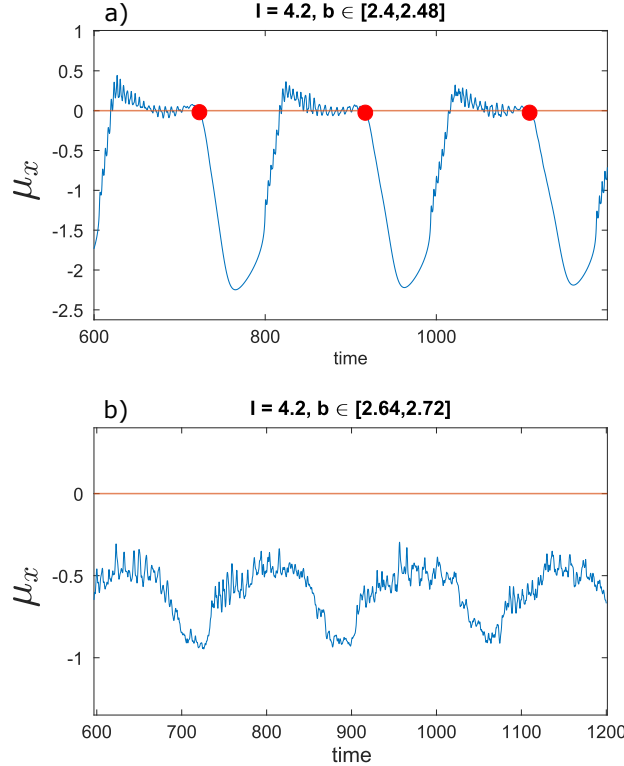


Figure 6: Expectation $\mathbb{E}[x] = \mu_x(t)$ for (a) the interval $b \in [2.4; 2.48]$, fully within regime D , and (b) $b \in [2.64; 2.72]$, fully outside regime D . μ_x was computed using the collocation method with $N_C = 15$ and $S_C = 400$. The red circles mark the end of the bursts of spikes at $\mu_x = 0$, for regime D (not happening for regime C).

4 Concluding Discussion

We have considered gPC methods as suitable candidates to accelerate probabilistic robustness studies, achieving a significant increase in efficiency with respect to Monte Carlo approaches and, in some cases, comparable accuracy.

We have considered both intrusive and non-intrusive gPC approaches, and collocation has been identified as an overall better approach for the study of neural dynamics. In particular, for systems in neuroscience, which are characterised by multiple complex regimes, the collocation method offers a good accuracy and significant improvement in efficiency compared to MC. By identifying how the statistics of the RMSE and the computational time depend on the polynomial order and the number of collocation points, our results also demonstrate the tradeoff between efficiency and accuracy, depending on the desired study objective.

We have demonstrated that in some cases a higher computational efficiency of the gPC approach with respect to MC is further accompanied by increased or comparable accuracy, thereby providing compelling evidence for the usefulness of gPC in the study of models in neuroscience. When the significant acceleration of the computation is accompanied by loss of accuracy, the method is still precious to identify regions of interest in the uncertain parameter space, where the resolution can be further refined by resorting to multi-element gPC, see e.g. [18]; this is an interesting direction for future research.

We considered models that range from single-neuron to interconnected neurons. A first case study of robustness for the Hindmarsh-Rose model confirms that the tuned collocation

method can rapidly identify the robustness region for the plateau bursting regime. The study highlights a transition point to alternative regimes that is consistent with the literature, and further supports the suitability of gPC surrogates to efficiently investigate complex models of biological interest. Future studies may expand the robustness analysis to all HR regimes and to other models, thus generating new insights into their robustness properties.

Acknowledgments

This work was funded by the European Union through the ERC INSPIRE grant (project number 101076926). Views and opinions expressed are however those of the authors only and do not necessarily reflect those of the European Union or the European Research Council Executive Agency. Neither the European Union nor the European Research Council Executive Agency can be held responsible for them.

References

- [1] Uri Alon. *An introduction to systems biology: design principles of biological circuits*. CRC, 2019.
- [2] Hiroaki Kitano. Towards a theory of biological robustness. *Mol Sys Biol*, 3, 2007.
- [3] Daniele Proverbio, Rami Katz, and Giulia Giordano. Bridging robustness and resilience for dynamical systems in nature. *IFAC-PapersOnLine*, 58(17):43–48, 2024. 26th International Symposium on Mathematical Theory of Networks and Systems MTNS 2024.
- [4] Stephanie K. Aoki, Gabriele Lillacci, Ankit Gupta, Armin Baumschlager, David Schweingruber, and Mustafa Khammash. A universal biomolecular integral feedback controller for robust perfect adaptation. *Nature*, 570:533–537, 2019.
- [5] Daniele Proverbio, Luca Gallo, Barbara Passalacqua, Marco Destefanis, Marco Maggiora, and Jacopo Pellegrino. Assessing the robustness of decentralized gathering: a multi-agent approach on micro-biological systems. *Swarm Int*, 14:313–331, 2020.
- [6] Mark S Goldman, Jorge Golowasch, Eve Marder, and LF Abbott. Global structure, robustness, and modulation of neuronal models. *J Neurosci*, 21(14):5229–5238, 2001.
- [7] Franco Blanchini and Giulia Giordano. Structural analysis in biology: A control-theoretic approach. *Automatica*, 126:109376, 2021.
- [8] B Ross Barmish. *New tools for robustness of linear systems*. Macmillan Publishing Company, 1994.
- [9] Roberto Tempo, Giuseppe Calafiore, and Fabrizio Dabbene. *Randomized algorithms for analysis and control of uncertain systems: with applications*, volume 7. Springer, 2013.
- [10] Nick Pepper, Francesco Montomoli, and Sanjiv Sharma. Multiscale uncertainty quantification with arbitrary polynomial chaos. *Comput Method Appl Mech Eng*, 357:112571, 2019.
- [11] Dongbin Xiu and George Karniadakis. The Wiener–Askey polynomial chaos for stochastic differential equations. *SIAM J Sci Comp*, 24(2):619–644, 2002.
- [12] Kwang-Ki K Kim and Richard D Braatz. Generalised polynomial chaos expansion approaches to approximate stochastic model predictive control. *Int J Control*, 86(8):1324–1337, 2013.
- [13] James Fisher and Raktim Bhattacharya. Optimal trajectory generation with probabilistic system uncertainty using polynomial chaos. *J Dyn Syst-T Asme*, 133:014501, 2011.

[14] Murray Rosenblatt. Remarks on a multivariate transformation. *Ann Math Stat*, 23(3):470–472, 1952.

[15] Ionut Florescu and Ciprian A Tudor. *Handbook of probability*. John Wiley & Sons, 2013.

[16] Norbert Wiener. The homogeneous chaos. *Am J Math*, 60(4):897–936, 1938.

[17] Robert Cameron and William Martin. The orthogonal development of non-linear functionals in series of fourier-hermite functionals. *Ann Math*, pages 385–392, 1947.

[18] Xiaoliang Wan and George Em Karniadakis. Multi-element generalized polynomial chaos for arbitrary probability measures. *SIAM J Sci Comp*, 28(3):901–928, 2006.

[19] Tom Lefebvre. On moment estimation from polynomial chaos expansion models. *IEEE Cont Sys Lett*, 5(5):1519–1524, 2020.

[20] Sergei Abramovich Smolyak. Quadrature and interpolation formulas for tensor products of certain classes of functions. In *Doklady Akademii Nauk*, volume 148, pages 1042–1045. Russian Academy of Sciences, 1963.

[21] Hermann Engels. *Numerical quadrature and cubature*. Academic Press, London, 1980.

[22] Felix Petzke, Ali Mesbah, and Stefan Streif. PoCET: a Polynomial Chaos Expansion Toolbox for Matlab. In *21st IFAC World Congress*, 2020.

[23] Dongbin Xiu. *Numerical methods for stochastic computations: a spectral method approach*. Princeton university press, 2010.

[24] Jeongeun Son and Yuncheng Du. Comparison of intrusive and nonintrusive polynomial chaos expansion-based approaches for high dimensional parametric uncertainty quantification and propagation. *Computers & Chemical Engineering*, 134:106685, 2020.

[25] James L Hindmarsh and RM Rose. A model of neuronal bursting using three coupled first order differential equations. *P Roy Soc B*, 221(1222):87–102, 1984.

[26] Giacomo Innocenti, Alice Morelli, Roberto Genesio, and Alessandro Torcini. Dynamical phases of the Hindmarsh-Rose neuronal model: Studies of the transition from bursting to spiking chaos. *Chaos: An Interdisciplinary Journal of Nonlinear Science*, 17(4), 2007.

[27] Arthur N Montanari, Leandro Freitas, Daniele Proverbio, and Jorge Gonçalves. Functional observability and subspace reconstruction in nonlinear systems. *Phys Rev Res*, 4(4):043195, 2022.

[28] Huaguang Gu. Biological experimental observations of an unnoticed chaos as simulated by the Hindmarsh-Rose model. *PLoS One*, 8(12):e81759, 2013.

[29] JM González-Miranda. Complex bifurcation structures in the Hindmarsh–Rose neuron model. *Int J Bif Chaos*, 17(09):3071–3083, 2007.

[30] Marco Storace, Daniele Linaro, and Enno de Lange. The Hindmarsh–Rose neuron model: bifurcation analysis and piecewise-linear approximations. *Chaos*, 18(3), 2008.

[31] Enno De Lange and Martin Hasler. Predicting single spikes and spike patterns with the Hindmarsh–Rose model. *Biol Cybern*, 99(4):349–360, 2008.

[32] Ben H Jansen and Vincent G Rit. Electroencephalogram and visual evoked potential generation in a mathematical model of coupled cortical columns. *Biological cybernetics*, 73(4):357–366, 1995.

[33] Viktor K Jirsa, William C Stacey, Pascale P Quilichini, Anton I Ivanov, and Christophe Bernard. On the nature of seizure dynamics. *Brain*, 137(8):2210–2230, 2014.

[34] Roberto Barrio and Andrey Shilnikov. Parameter-sweeping techniques for temporal dynamics of neuronal systems: case study of Hindmarsh–Rose model. *J Math Neurosci*, 1:1–22, 2011.